Biophysical Chemistry 251 (2019) 106190

Contents lists available at ScienceDirect

Biophysical Chemistry

journal homepage: www.elsevier.com/locate/biophyschem

Single-molecule insights into the temperature and pressure dependent conformational dynamics of nucleic acids in the presence of crowders and osmolytes

Loana Arns[a], Jim-Marcel Knop[a], Satyajit Patra[b], Christian Anders[a], Roland Winter[a,*]

[a] TU Dortmund University, Faculty of Chemistry and Chemical Biology, Physical Chemistry, Otto-Hahn-Str. 4a, D-44227 Dortmund, Germany
[b] Aix Marseille Université, CNRS, Centralle Marseille, Institut Fresnel, F-13013 Marseille, France

HIGHLIGHTS

- The conformation of DNA and RNA hairpins is markedly affected by macromolecular crowders and organic osmolytes.
- Specific compatible osmolytes are able to alleviate deteriorating effects of high pressure, high temperature and urea.
- Artificial macromolecular crowders, such as Ficoll, may not act as inert crowding agents.
- The effects of osmolytes and crowders dependent on the structure and chemical make-up of the nucleic acid.

GRAPHICAL ABSTRACT

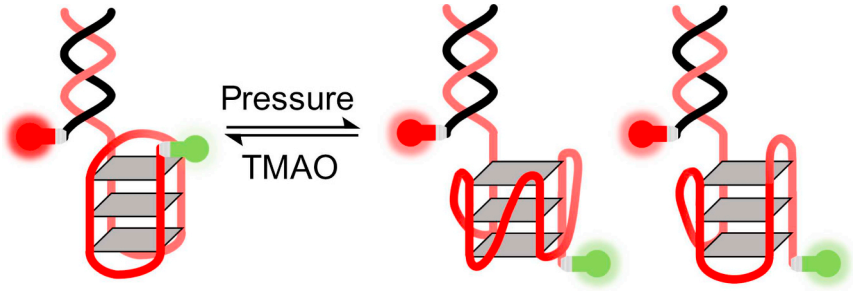

ARTICLE INFO

Keywords:
High pressure
Crowding
Osmolytes
Nucleic acids
Conformational dynamics
Single-molecule FRET

ABSTRACT

In this review we discuss results from temperature and pressure dependent single-molecule Förster resonance energy transfer (smFRET) studies on nucleic acids in the presence of macromolecular crowders and organic osmolytes. As representative examples, we have chosen fragments of both DNAs and RNAs, i.e., a synthetic DNA hairpin, a human telomeric G-quadruplex and the microROSE RNA hairpin. To mimic the effects of intracellular components, our studies include the macromolecular crowding agent Ficoll, a copolymer of sucrose and epichlorohydrin, and the organic osmolytes trimethylamine *N*-oxide, urea and glycine as well as natural occurring osmolyte mixtures from deep sea organisms. Furthermore, the impact of mutations in an RNA sequence on the conformational dynamics is examined. Different from proteins, the effects of the osmolytes and crowding agents seem to strongly dependent on the structure and chemical make-up of the nucleic acid.

1. Introduction

The deep sea is the largest habitat on Earth, challenging living organisms to adapt to extreme environmental conditions. The predominant stress factor is high hydrostatic pressure (HHP), which increases by 1 bar for each 10 m in depth. Alteration of pressure affects biochemical processes and equilibria that are accompanied by molar volume changes, ΔV, of the biomolecules including their hydration layer. Hence the effect of high pressure is dependent on the sign and magnitude of ΔV. In deep sea organisms, a variety of strategies to counteract the deleterious effects of pressure evolved. In addition to intrinsic adaptations, such as changes in the amino-acid sequence of

* Corresponding author.
E-mail address: roland.winter@tu-dortmund.de (R. Winter).

https://doi.org/10.1016/j.bpc.2019.106190
Received 30 April 2019; Received in revised form 20 May 2019; Accepted 20 May 2019
Available online 23 May 2019
0301-4622/ © 2019 Elsevier B.V. All rights reserved.

proteins, there is evidence that extrinsic adaptation by the accumulation of organic osmolytes is a widespread strategy in deep sea fishes [1]. However, molar volume changes are also affected by the excluded volume effect imposed by high concentrations of biomacromolecules present in the cytoplasm. In such a crowded environment, only a limited space is available for a particular biomolecule. Therefore, in vitro measurements carried out in a dilute buffer may not accurately mimic intracellular conditions. Additionally, crowding increases the viscosity of the medium and therefore decreases the molecular motions and diffusion-controlled kinetics [2–4]. Previous reports have shown that the excluded volume effect significantly affects the kinetics of association reactions, the folding behavior of proteins and RNAs and the compactness of intrinsically disordered proteins [5–7].

The interaction mechanism of osmolytes with nucleic acids is less universal than the preferential binding / exclusion mechanism generally discussed for osmolytes with proteins. The underlying interactions are strongly dependent on the physicochemical properties of the cosolute. Favorable and accordingly unfavorable interactions are strongly dependent on the affinity to the different nucleotide building blocks, i.e., the nucleobases, (deoxy-)ribose and phosphate groups. For instance, the protein stabilizing osmolyte trimethylamine-*N*-oxide (TMAO) was found to effectively stabilize tertiary structures of RNA and DNA due to unfavorable interactions with exposed phosphate groups, while it seems to exhibit weak protection abilities for secondary structures [8,9]. However, favorable interactions between osmolytes and nucleobases may shift the double-stranded DNA (dsDNA) vs. single-stranded DNA (ssDNA) equilibrium to the formation of the ssDNA [10,11]. It was found that some osmolytes alter the concentration of counterions at the DNA-solvent interface, resulting in a modification of the water dynamics of the DNA's hydration shell [12,13]. Additionally, certain osmolytes may show different affinities to A and T bases and to G and C bases, respectively [14,15]. Thus, the percentage of the AT and GC content of the DNA under investigation is a further aspect that has to be taken into account in characterizing the origin of stabilizing or destabilizing effects of osmolytes.

Previous high-pressure studies on the conformational stability of nucleic acids revealed that canonical B-DNA duplex structures are generally stabilized with increasing pressure [16–19]. High pressure promotes base stacking and reduces the length of Watson-Crick hydrogen bonds. Therefore, the distance between A and T is reduced more effectively then between G and C, as they are stabilized by two and three hydrogen bonds, respectively [20]. Furthermore, DNA helix geometries may be modulated upon pressurization. Reorientations between the B-DNA form and the Z-DNA form or A-DNA form have been discussed at elevated pressures [21–23]. Other non-canonical structure motifs like G-quadruplexes or hairpins seem to be rather pressure sensitive, but it was shown that the sensitivity depends on the counterion concentration and base sequence [24–28].

As crowders and osmolytes are prone to alter the conformation and dynamics of biomolecules, a large number of studies concerning the elucidation of the underlying mechanisms have been reported. However, these studies are mainly focusing on proteins [28–35], and only very recent studies on crowding and osmolyte effects on nucleic acid structures gained momentum [4,9,36–41]. However, quantification of crowding and osmolyte effects on the conformational dynamics of nucleic acids on the single-molecule level is still largely unexplored [4,9,36,39]. Single-molecule FRET (smFRET) is a very powerful technique in deciphering the conformation and conformational dynamics of biomolecules as it provides information which is not averaged out as in an ensemble measurement. The smFRET technique can distinguish between intermediate states or transient conformers and fully folded and unfolded states, and additionally allows to study their dynamics [42,43]. A temperature and pressure variable smFRET study can provide detailed insights into the thermodynamics and volumetric profiles of the conformational transitions of nucleic acids, which is otherwise inaccessible.

In this review, we will discuss some of our recent results and present new data of pressure and temperature dependent smFRET studies on nucleic acids in the presence of macromolecular crowders and organic osmolytes. We have chosen fragments of both DNA and RNA, a synthetic DNA hairpin, a human telomeric G-quadruplex and the microROSE RNA hairpin. To mimic the effects of intracellular components, our studies include the macromolecular crowding agent Ficoll, a copolymer of sucrose and epichlorohydrin, and the organic osmolytes TMAO, urea and glycine as well as natural occurring osmolyte mixtures from deep sea organisms.

2. Methods

2.1. Single-molecule FÖRSTER resonance energy transfer (smFRET)

All smFRET measurements were performed on a commercial time-resolved confocal fluorescence microscope (PicoQuant, MicroTime 200). Details of the setup can be found elsewhere [4]. The pulsed interleaved excitation FRET (PIE-FRET) technique was used for all the smFRET studies. In classical smFRET, the donor-only fraction generally leads to an artificial low-FRET peak, typically around 0.1–0.2 in the FRET efficiency (E_{FRET}) histograms, rendering the characterization of the low-FRET species impossible [44]. The PIE-FRET technique can filter out the dually labeled species from the singly labeled (donor-only and acceptor-only) species [45]. Briefly, in PIE-FRET two lasers are chosen with suitable wavelength to excite both donor and acceptor separately. The laser pulses are delayed with respect to each other such that the fluorescence due to donor excitation appears in the early time window and the fluorescence due to direct excitation of the acceptor appears in the later time window. This information is used to determine the photon stoichiometry, *S,* which is defined as the ratio of the photons emitted due to donor excitation and the sum of the total emitted photons due to both donor and acceptor excitation. For the donor- and acceptor-only fraction, the value of *S* is 1 and 0 respectively. Singly labeled species are thus excluded from the photons used to calculate the FRET efficiency. Pulsed diode lasers (LDH series, PicoQuant) of wavelength 560 nm and 635 nm with repetition rate 20 MHz were used to excite the donor (Atto 550) and acceptor (Atto 647 N) fluorophore, respectively. The output of the green and red laser is coupled to the main optical unit by using a polarization maintaining single mode optical fiber. In the main optical unit, the green and red laser is guided through a quad band dichroic mirror (ZT 405/488/561/640, Chroma) which reflects the excitation beam into the entrance port of the microscope. A water immersion objective (UplansApo, 60X, 1.2 NA) in the microscope focuses the excitation beam on the solution drop placed on a coverslip. The fluorescence is collected in the same path, passed through the dichroic mirror, 575 nm long pass filter (HQ 575 LP, Chroma), the spatially filter by a 50 μm pinhole, and is finally spectrally separated into two detection channels using a dichroic mirror (FF 650 Di 01, Semrock). To further suppress the spectral leakage, two band pass filters FF01-593/40 and FF01-676/29 are used in front of the donor and acceptor detection channel, respectively. Two SPCM-AQR series single photon avalanche diodes (SPAD) are used to detect the donor and acceptor fluorescence. Each photon is stored with individual timing and channel information using a time-correlated single photon counting unit with the TimeHarp 200 PCI board in a Time-Tagged-Time resolved mode. All the diffusion based smFRET measurements were carried out at an excitation power of 12 μW.

2.2. High-pressure smFRET setup

All smFRET measurements at high pressure were carried out under freely diffusing conditions in a square-shaped flexible fused silica microcapillary with outer diameter 360 μm and inner diameter 50 μm. In this case, the capillary serves both as a mechanical body and optical window of the high-pressure cell. The optical window thickness of this

capillary is 150 µm, which resembles standard coverslip thicknesses used in fluorescence microscopy studies. A detailed description of the high-pressure cell including its optimization and optical characterization is provided in a recent report by us [46]. Briefly, first the polyimide coated capillary is glued into a high-pressure plug with the help of two component epoxy glue. Then, an optical window is prepared at the appropriate location of the capillary where it meets the objective lens by just burning off a small section of the polyimide coating using a lighter. The sample solution is sucked into the capillary and the free end is flame-sealed using an oxygen propane blow torch. Next, the pressure plug is placed in the microscope stage using a specially designed aluminum plate. Finally, the pressure plug end of the capillary is connected to the high-pressure flexible tube using a metal coupling unit for pressure generation. The metal coupling unit is placed on a translation table which is position-controlled by horizontal, vertical and turning screws for fine-tuning the position of the capillary.

2.3. Annealing of the DNA strands

For annealing, the oligonucleotide strands (for hairpin H2, A2 and for the G-Quadruplex G and C) are mixed in a 1:1 ratio in a buffer containing 20 mM Tris-HCl, 50 mM NaCl, at pH 7.5. The mixture is first heated at 95 °C for 5 min and then gradually cooled down to room temperature at a rate of −0.5 °C/min using a thermocycler.

2.4. Sample preparation of the microROSE RNA hairpin

The wildtype (WT) microROSE and mutant (ΔG83) were custom synthesized by IBA (Göttingen, Germany). The sequences of the hairpins are WT: GGCC AUCU UGCU CUUC GGAG GAUU UGGCC and ΔG83: GGCC AUCU UCUC UUCG GAGG AUUU GGCC. For the ensemble and single-molecule FRET measurements, the strands were labeled with Atto 550 (NHS-ester) via a C6 amino linker at the 5′-terminus, and the 3′-terminus was labeled with Atto 647N via click chemistry using C8-alyne-dC by IBA as well. The additives TMAO, glycine and sucrose were purchased from Sigma Aldrich (Germany). Ficoll™ PM70 was obtained from GE Healthcare (Uppsala, Sweden).

All solutions were prepared in 15 mM Tris-HCl buffer (pH 7.4) and filtered through a 0.02 µm Whatman Anotop™ 25 Plus syringe filter (GE Healthcare Life Sciences, Germany). Salt concentration dependent measurements were performed with 25 mM, 100 mM and 150 mM KCl in buffer. All measurements in the presence of additives were performed at a salt concentration of 100 mM KCl.

Lyophilized RNA samples were dissolved in the particular buffer solution and kept at 95 °C for 10 min, followed by snap-freezing in liquid nitrogen to obtain a homogenous population of monomeric stem loops.

2.5. Analysis of the smFRET data under freely diffusing condition

Extremely low concentrations of the sample (50–300 pM) ensure that the probability of having more than one molecule in a ~1 fL confocal volume is extremely low. Each transit of a single molecule through the confocal volume generates a characteristic fluorescence signal, also called fluorescence burst, due to a multiple excitation and emission cycle. The duration of each burst is equal to the diffusion time of the molecule. A threshold is used to separate these fluorescence bursts from the background signal. A second threshold criterion is used to select the fluorescence bursts for the calculation of the FRET efficiency. Only when the sum of the donor and acceptor photons in a time bin is greater than the threshold value, it is considered as a single-molecule event [47]. In our measurements, the second threshold value is kept at 25 photons. The photons in each selected burst are used to calculate the FRET efficiency, E, which is defined as

$$E = \frac{n_A}{n_A + \gamma n_D} \quad (1)$$

where n_A and n_D is the number of photons in the acceptor and donor channel, respectively, and γ takes into account the different fluorescence quantum yields and detection sensitivities of the donor and acceptor. We estimated $\gamma = 0.88$ in our set up for the donor-acceptor pair Atto 550 and Atto 647 N. Eq. (1) needs still to be corrected in order to avoid experimental artefacts in the FRET analysis, such as leakage of donor emission in the acceptor channel and direct excitation of the acceptor emission at donor excitation. The corrected FRET efficiency is defined as

$$E = \frac{n_A - \alpha n_D - \beta n_A^{red}}{(n_A - \alpha n_D - \beta n_A^{red}) + \gamma n_D} \quad (2)$$

Here, α is the correction factor for the crosstalk and is defined as the ratio of donor-only fluorescence leaked into the acceptor channel and donor-only fluorescence detected in the donor channel. β takes into account the direct excitation of the acceptor emission at donor excitation and is defined as the ratio of acceptor-only emission obtained in the acceptor channel at donor excitation and the acceptor-only emission in the acceptor channel due to excitation at red wavelength (n_A^{red}). In our setup we have estimated $\alpha = 0.05$ and $\beta = 0.08$.

3. Results and discussion

3.1. Effect of low temperature and high pressure on the conformational equilibrium of a DNA hairpin in the presence of a natural osmolyte mixture

As a first example, we present a study of the pressure-induced helix-to-coil transition of a synthetic DNA hairpin (DNA hp) at 4 °C and 20 °C in the absence and in the presence of a naturally occurring osmolyte mixture found in deep sea shrimps. The mixture contains mainly TMAO and glycine and small amounts of betaine and valine only (Fig. 1B) [46,48]. The hairpin consists of two complimentary oligonucleotide strands and a A_{32} loop (Fig. 1A) [49]. The stem is labeled with Atto 550 close to the loop and with Atto 647 N toward the 5′-end to yield a donor-acceptor pair for smFRET measurements. The position of the two dyes provides sufficient differences in FRET efficiencies (80% in the closed state, 20% in the unfolded state) to detect the unfolding transition of the DNA hp with high accuracy. The huge size of the loop ensures conformational flexibility so that the hairpin may serve as a

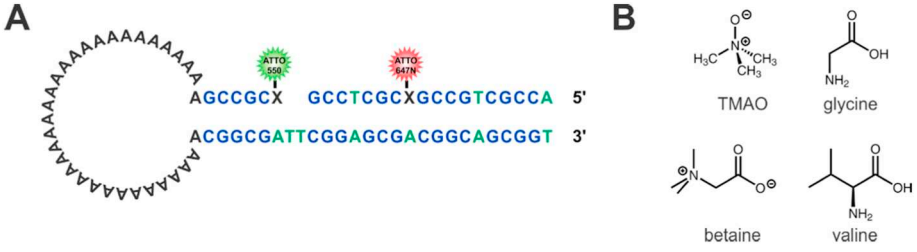

Fig. 1. (A) Chemical structure of the DNA hairpin (X = T) [50]. The FRET pair Atto 550 and Atto 647 N is attached to the stem. (B) Chemical formula of the osmolytes present in the deep sea shrimp osmolyte mixture [48].

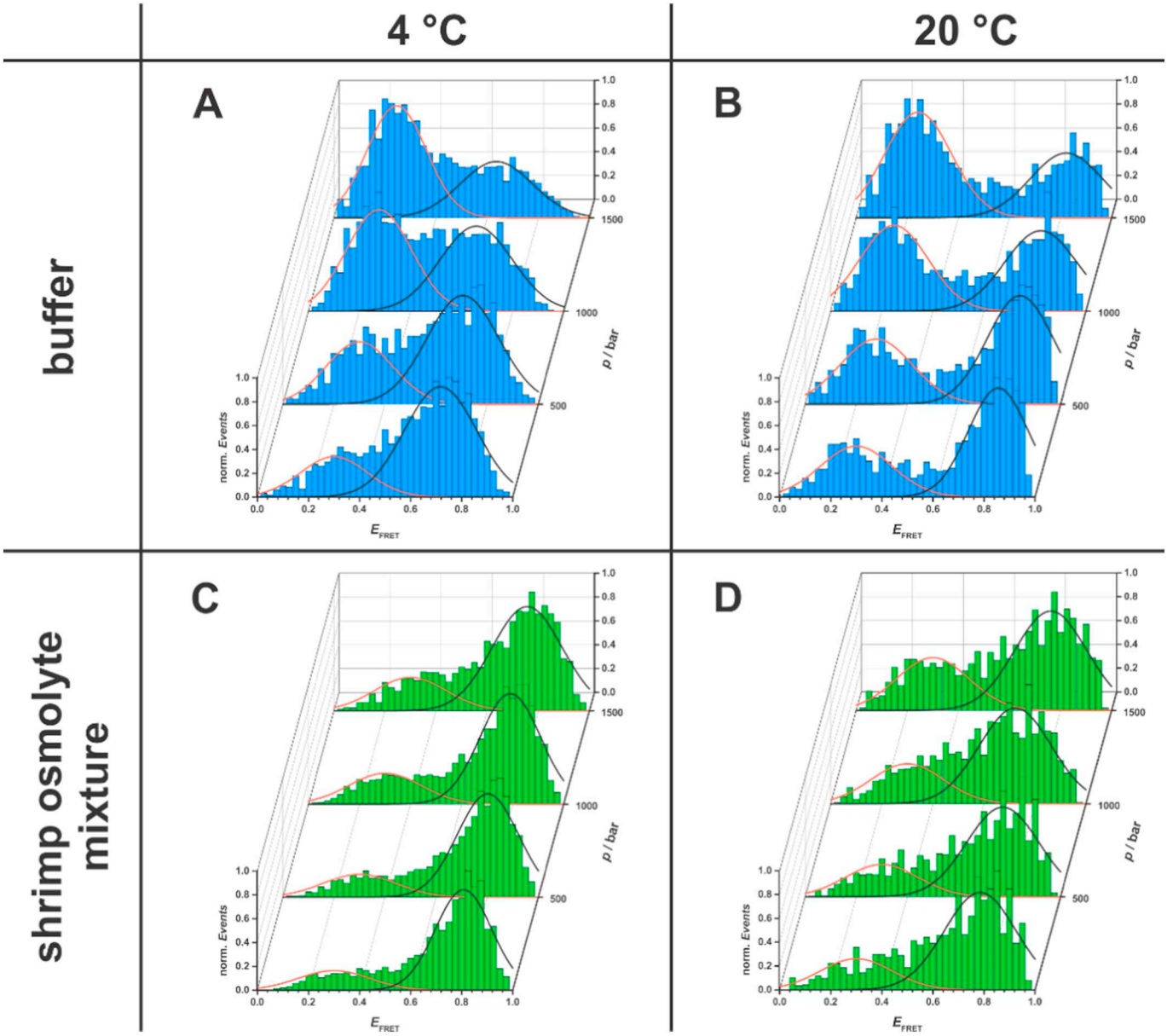

Fig. 2. Effect of pressure on the helix to coil transition of the DNA hairpin in neat buffer (A,B) and a shrimp osmolyte mixture (C,D) at low and ambient temperature. Data presented in B and D are reproduced from Patra et al. 2018 [46] with permission from the PCCP Owner Societies. The protective effect of the DS mix is increased at the lower temperature.

convenient probe for detection of conformational changes induced by pressure, temperature and cosolute changes. Previous studies on this DNA hp have been published recently [4,46].

Fig. 2 presents the FRET efficiency (E_{FRET}) histograms gained from the pressure dependent smFRET measurements of the DNA hp under free diffusion conditions. For better comparability, the histograms were fitted to a bimodal Gaussian distribution representing two conformational species with different FRET efficiencies. The peak at low E_{FRET} is related to a coiled conformation, where the duplex strand adjacent to the loop is open. The second, high E_{FRET} species represents the closed conformation of the DNA hp. Interestingly, some histograms offer evidence for the existence of intermediate states with medium FRET efficiency. From the peak areas, we determined the fraction of the open and closed conformation present at each pressure amplitude. The increase of the percentage of the open conformation with increasing pressure is presented in Fig. 3.

We found that over the whole pressure range covered (1–1500 bar), the hairpin is always in an equilibrium between the open and close conformation, not exhibiting 100% of one state in any case. At ambient pressure and temperature (1 bar, 20 °C; Fig. 2B), the closed conformation is favored with a closed-to-open ratio of about 1.6:1. Upon pressurization, the equilibrium is shifted to the low-E_{FRET} species, being balanced (1:1) at 1 kbar and reversed (1:1.6) at 1.5 kbar. As high hydrostatic pressure generally stabilizes DNA duplex structures, we assume that the shift to lower FRET efficiencies, indicating an increasing distance of the two dyes, is initiated by a destabilization of the stem region adjacent to the loop. We found a negative volume change upon unfolding, $\Delta V = -19.6 \pm 1.3\,cm^3\,mol^{-1}$ for the pressure-induced opening of the hairpin, indicating a lower partial molar volume of the open conformer. Hence the equilibrium between the closed and open state is shifted toward the open state upon pressurization.

Cooling the system to 4 °C (Fig. 2A) reduces the separation of the two FRET efficiency peaks, which suggests the formation of intermediate conformational states with medium FRET efficiency, but might also be due a decreased rate of interconversion between the open and close conformation. Analysis of the fraction of low-E_{FRET} species,

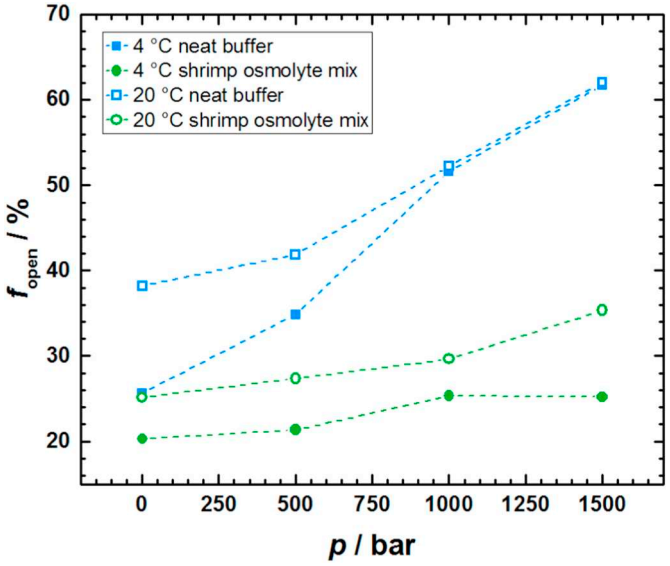

Fig. 3. Pressure dependent increase of the percentage of the open conformation of the DNA hp. in neat buffer (blue) and a shrimp osmolyte mixture (green) at low (4 °C) and ambient temperature (20 °C, data are reproduced from Patra et al. 2018 [46] with permission from the PCCP Owner Societies). (For interpretation of the references to colour in this figure legend, the reader is referred to the web version of this article.)

compared to the 20 °C data, reveals that the fraction of open conformers is slightly lower at 4 °C and ambient pressure, which might be due to a faster folding rate, but increases to the same percentage upon pressurization up to 1.5 kbar (Fig. 3, open and closed blue squares).

Deep sea organisms accumulate a variety of organic osmolytes to counteract the deleterious effects of high hydrostatic pressures. Our smFRET studies of the DNA hp in the presence of a deep sea shrimp osmolyte mixture (DS mix) indicate a drastic stabilization against unfolding of the DNA hp. over the whole pressure range covered. Comparing the measurements at low and ambient temperature (Fig. 2C and D; Fig. 3, green dots) reveals that this effect is even more pronounced at 4 °C, the temperature prevailing in the deep sea. The DS mix contains 590 mM TMAO, 100 mM glycine, 35 mM betaine and 20 mM valine. Our previous studies carried out at 20 °C revealed that the marked stabilizing effect of the osmolyte mixture is provoked by the major component of the DS mix, i.e. TMAO [46]. While TMAO was shown to destabilize RNA secondary structures but to stabilize RNA tertiary structures, Holmstrom et al. found a stabilizing effect for both secondary and tertiary structures of DNA [8,9]. In temperature dependent smFRET measurements, an entropic destabilization of the unfolded state was found to be the reason for the thermodynamic preference for the duplex of a short DNA strand in the presence of TMAO. Additionally, we found the volume change upon unfolding to be drastically reduced to $-7.8 \pm 0.9\,cm^3\,mol^{-1}$ in the presence of 1 M TMAO at 20 °C, indicating a more compact unfolded state structure [4]. For the following reasons we surmise that the volumetric properties of the hairpin are mainly determined by the A_{32} loop. In former volumetric studies on DNA hairpins with smaller loops (4 bases), the ΔV was found to be in the range of -2.35 to $+6.74\,cm^3\,mol^{-1}$, depending on the salt concentration and on temperature [27]. The rather high ΔV value of our DNA hp indicates packing defects of the adenine bases in the folded state that might create void volumes which are filled with water molecules upon unfolding. The decrease of ΔV in the presence of TMAO could either indicate a more compact folded or unfolded state. A more compact unfolded state should be accompanied by a shift of the low E_{FRET} peak to higher FRET efficiencies, which was not observed in our recent study [4]. Hence, the large A_{32} loop of the closed conformation might be forced to a more compact conformation due to unfavorable interactions between TMAO and the phosphate groups of the DNA backbone [8], i.e. due to the strong excluded volume effect TMAO imposes on the biomolecule, leading to less internal voids and concomitantly a smaller volume change upon unfolding.

3.2. High-pressure studies on a G-quadruplex in the presence of osmolytes and crowding agents

First observed *in vitro* and taken for an artifact, interest in stacked guanidine tetrads raised after the discovery of G-quadruplex (G-Qdp) formation in guanidine-rich telomere DNA and some promotor regions of oncogenes (e.g., cMyc) [50–52]. The strategy of single-stranded DNA overhang for chromosome stabilization against the limits of DNA duplication is not exclusive for mammalians and can also be found, for example, in fish [53]. Since then, many studies started to characterize the topology of DNA G-Qdp depending on temperature, pressure, salt concentration, DNA length and nucleobase composition [24,54–56]. While CD, fluorescence and NMR spectroscopies were used to observe structural changes of the ensemble of molecules, e.g. unfolding with increasing temperature and pressure, insights into the conformational substates is provided by methods with single-molecule resolution, such as by smFRET microscopy of double-labeled DNA oligomers [37,57,58]. Based on these methods, an amazingly large conformational diversity was uncovered, characterized by the direction of the G-strands and their connection. NMR has the advantage of atomic resolution, biased by the necessity of having to use rather high concentrations (mM range), however. Orthogonal results can be obtained by smFRET measurements, which provide only intramolecular distances and need to be assigned to different conformations, but work at very low concentrations (pM range). Today, G-Qdps are sub-classified into parallel, antiparallel and hybrid forms. Schematic examples of conformations are depicted in Fig. 4.

We studied the conformational changes of a 38 nucleobases long construct, consisting of the human telomeric sequence (hTel23), known for G-Qdp formation [59] and a 15 nucleobases long double strand (Fig. 5a), up to pressures of 1.5 kbar and at temperatures up to 80 °C. Furthermore, the influence of TMAO and urea as well as the macromolecular crowder Ficoll 70 were added at low salt concentration conditions (5 μM NaCl). FRET efficiency histograms were fitted with a three Gaussian model, integrated and normalized to obtain the relative FRET populations, which were assigned to antiparallel (high $E_{FRET} \approx$

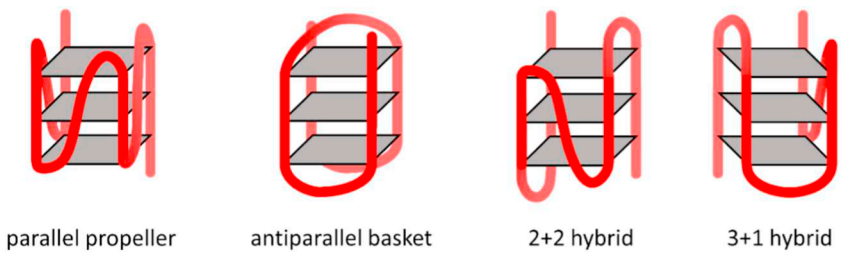

Fig. 4. Schematic examples of G-quadruplex conformations. For example, the parallel propeller was observed in cMyc promotor, the antiparallel basket in telomeric sequences *in vivo*, and hybrid conformations *in vitro* at distinct salt and crowder conditions [50,57–59].

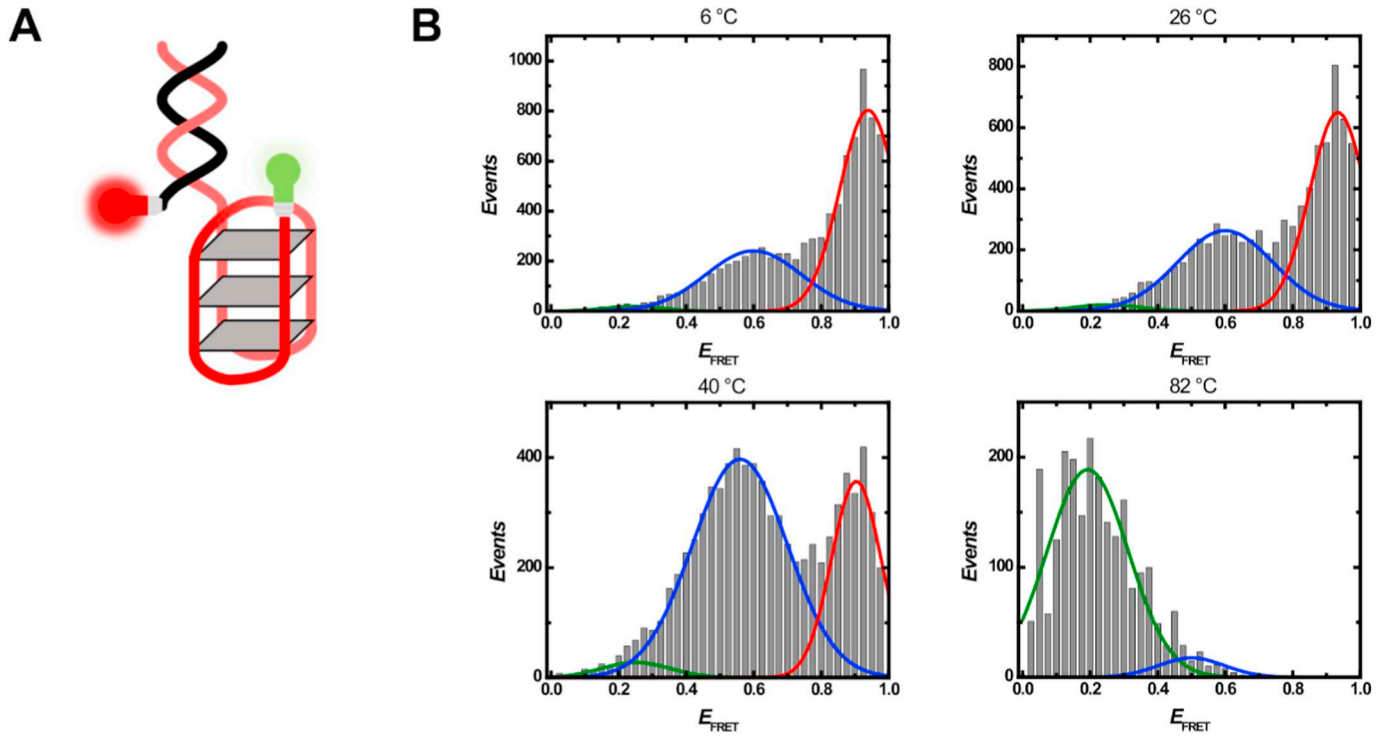

Fig. 5. (A) Scheme of the investigated DNA G-quadruplex construct labeled with Atto 550 (green bulb) and Atto 647 N (red bulb) in an antiparallel (high E_{FRET}) state. (B) Exemplary histograms of temperature-dependent PIE smFRET measurements in neat buffer at different temperatures and ambient pressure. The curves of the three-Gaussian fit represent the following conformations: red: high E_{FRET}, antiparallel conformation; blue: medium E_{FRET}, parallel/hybrid conformation; green: low E_{FRET}, random coil. (For interpretation of the references to colour in this figure legend, the reader is referred to the web version of this article.)

0.8), parallel/hybrid (medium $E_{FRET} \approx 0.6$) and unfolded (low $E_{FRET} \approx 0.3$) conformations.

Fig. 5B depicts a representative example for fitted histograms of temperature dependent measurements at ambient pressure. In the low temperature range between 6 °C and 25 °C, the population of the antiparallel structure does not change significantly (Fig. 6A). Upon further increasing the temperature, the parallel/hybrid conformation becomes predominant (around 33 °C), similar to the effect of high pressure (see below). At $T_m = 54 \pm 1.5$ °C, unfolding of the G-Qdp is observed. The parallel conformation has a higher SASA and therefore a higher amount of hydration water. As a result, the hydration contribution to the enthalpy and entropy change, ΔH_{H_2O} and ΔS_{H_2O}, are suggested to be negative with the entropic part becoming more important at higher temperatures. This leaves the contribution of the quadruplex conformational changes to be responsible to yield a negative ΔG at higher temperature, possibly owing to a more flexible structure of the parallel/hybrid conformation compared to the antiparallel one.

The pressure dependent studies revealed a pressure-induced change of the DNA G-Qdp structure from an antiparallel to a parallel/hybrid conformation with a transition pressure of 400 ± 150 bar, which is accompanied by a volume change of $\Delta V = -26.2 \pm 0.5\,cm^3\,mol^{-1}$ for this conformational transition. Further increase of pressure leads to unfolding of the G-Qdp (Fig. 6B). The initial conformational change from the antiparallel basket conformation to the hybrid or parallel conformation upon compression could be explained by the lower solvent accessible surface area (SASA) of the antiparallel conformation [60], leading to increased hydration upon pressurization. This effect is suggested to be driven by the lower molar volume of hydration water compared to bulk water [37,61]. The pressure effect is counteracted by 1 M TMAO or 15 wt% Ficoll 70. Additionally, the relative population of the antiparallel conformation at ambient conditions is increased (Fig. 6 D and C). The stabilization of the antiparallel conformation of the G-Qdp by 1 M TMAO can be explained by unfavorable interactions between TMAO and the nucleobases as well as the phosphate-backbone. In case of TMAO, the volume decrease is smaller ($\Delta V = -17.0 \pm 0.3\,cm^3\,mol^{-1}$). Owing to a strong excluded volume effect, the macromolecular crowding agent Ficoll 70 favors more compact conformations with lower SASA as well [30]. Urea has an opposite effect: 2 M urea leads to unfolding at ambient conditions. The favorable interaction of urea and nucleobases is considered responsible for its destabilizing effect, finally leading to unfolding at sufficiently high concentrations, i.e. urea shifts the equilibrium toward conformations with a higher SASA (Fig. 6E) [62,63]. A mixture of 1 M TMAO and 2 M urea leads to the initial population of the conformers observed in neat buffer solution (Fig. 6B and F). With increasing pressure, a slight increase of parallel and unfolded states appears above 500 bar, finally reaching a relative population of 42% parallel, 35% antiparallel and 23% unfolded states. This can be rationalized invoking an overcompensation of the deteriorating effect of urea, with TMAO still able to rescue a predominant fraction of the G-Qdp from unfolding at 1.5 kbar (Fig. 6F) [37].

In conclusion, for adaptation to extreme conditions like HHP or high temperatures, it is not only necessary to maintain the function of the protein machinery, but also to stabilize non-canonical conformations of nucleic acids needed for proper epigenetic regulation. We have seen that particular osmolytes, such as TMAO which is upregulated in deep sea organisms, are able to rescue native structures of telomeric G-Qdp even at pressures up to about 800 bar.

3.3. Temperature dependent conformational changes of an RNA thermometer in the presence of osmolytes and crowders

Biochemical processes are sensitive to environmental stress factors like heat or cold, drought, hydrostatic pressure or high salinity. In the course of evolution, several strategies to respond to those stresses evolved in living organisms. For instance, in bacteria the expression of heat shock genes is induced when the temperature reaches a critical level. The translation is controlled by a temperature-sensitive conformational change in mRNAs, referred to as RNA thermometers [64].

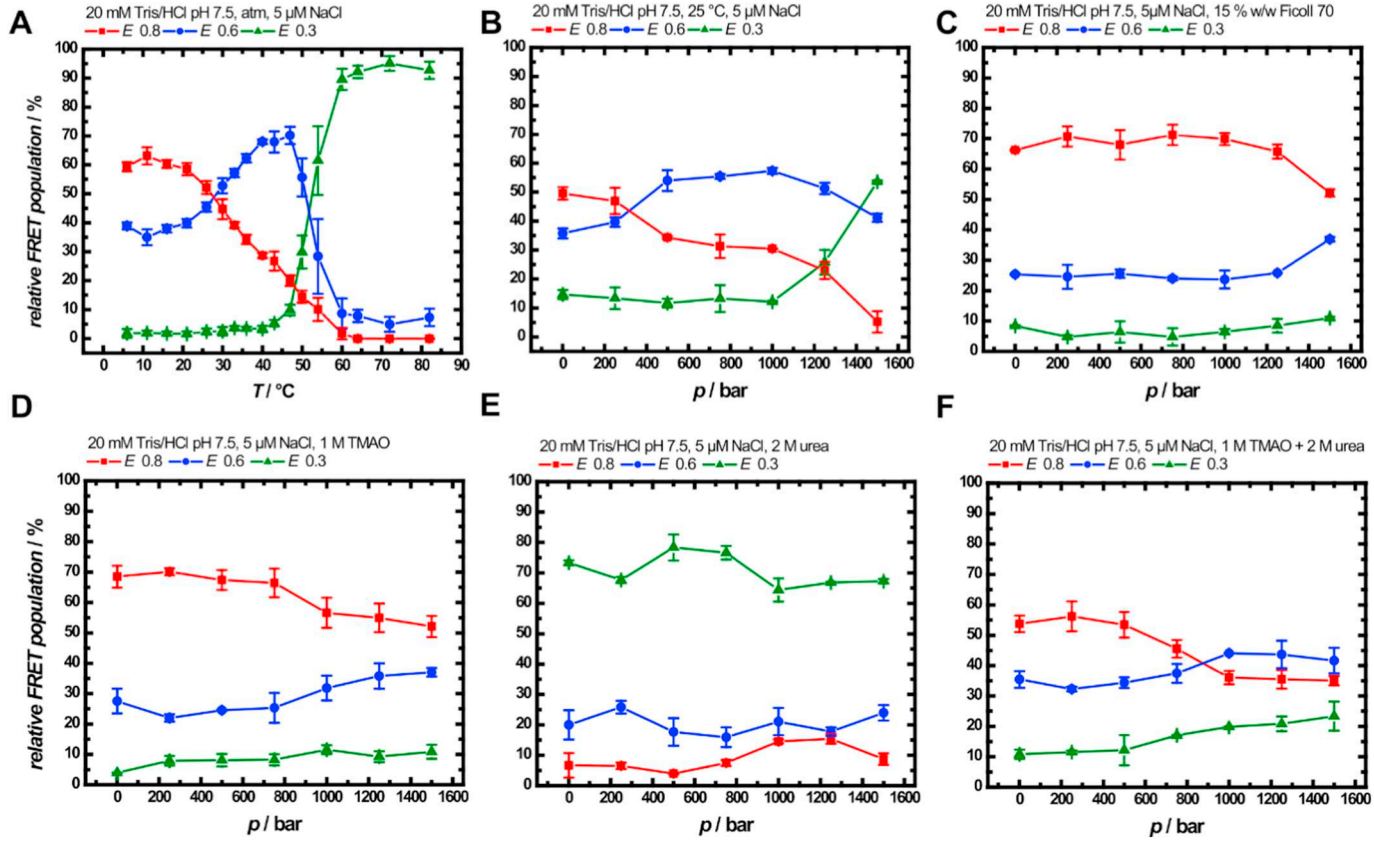

Fig. 6. Pressure dependent FRET population of the double labeled G-Qdp construct in different solutions containing 5 µM NaCl, 20 mM Tris/HCl pH 7.5 and different cosolvents or crowders. Measurements were performed at 25 °C. Data are reproduced from [37] with permission from John Wiley and Sons. Ficoll and TMAO promote the formation of the antiparallel conformation (high FRET efficiency, $E_{FRET} \approx 0.8$), while urea induces unfolding of the G-Qdp.

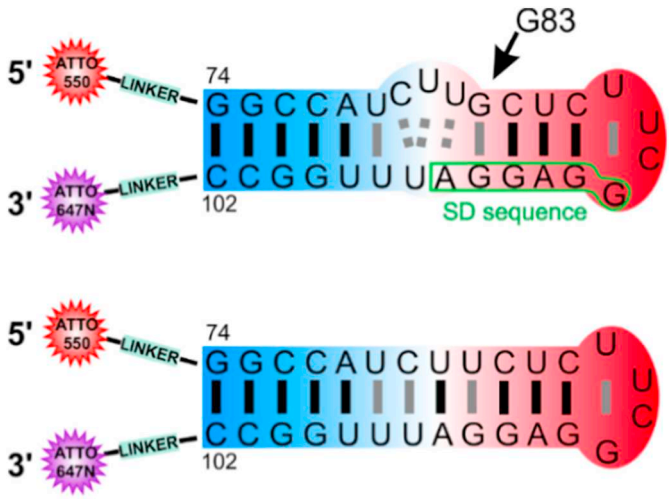

Fig. 7. Chemical structures of the wildtype (top) and ΔG83 mutant (bottom) of the microROSE RNA hairpin.

In a zipper-like mode, hydrogen bonds between base pairs are broken as temperature increases. Once the AUG start codon is fully accessible to the initiator tRNA, translation commences before thermal induced damaging of cellular components can occur. As cellular background molecules generally have an impact on the conformational dynamics of biomolecular structures, the conformational properties and stabilities of RNA thermometers are expected to be affected as well. The thermosensing ROSE element (repressor of heat-shock gene expression) is a mRNA which consists of four consecutive hairpins [65]. We have chosen the SD sequence containing microROSE hairpin (29 bases) located at the 5′ end of the thermometer to explore the effect of salts, osmolytes and crowders on its temperature dependent conformational changes. The hairpin possesses an internal loop that is located next to the SD sequence (Fig. 7, top). The internal loop is essential for the thermosensing [64,65]. Based on the studies of Chowdhury et al., we have included a mutant of the microROSE hairpin in the salt concentration dependent studies. The mutant is lacking the internal loop as a result of the deletion of G83 (Fig. 7, bottom) and has consequently no thermosensing properties. We expected the perfectly matched secondary structure of the ΔG83 mutant to be more temperature stable and used smFRET experiments to gain detailed insights into the stability and conformational dynamics of the microROSE RNA hairpin upon addition of selected cell-like background molecules.

Osmolytes such as TMAO generally stabilize the native state of proteins by an indirect mechanism, i.e., interactions of TMAO with water are more favorable than interactions with the protein's solvent accessible surface area (SASA) [34,66,67]. The effect of TMAO on nucleic acids is less universal. Lambert et al. found that the osmolyte stabilizes tertiary structures of RNAs while secondary structures are slightly destabilized [8,41]. Destabilization may be related to hydrogen bonding of TMAO with the nucleobases [68,69]. Macromolecular crowders are generally thought to stabilize compact folded structures due to the excluded volume effect. However, destabilization may be provoked by enthalpically driven soft attractive interactions of the biomolecule with the crowding agent [70]. For the folding equilibria of proteins, the excluded volume effect was often found to be predominant [71]. In the case of RNAs, the mode of action is more diverse. Crowding agents like PEG (polyethylene glycol) and Ficoll seem to stabilize tertiary and quaternary structures, while secondary structures have been shown to be destabilized [35,72,73]. Our FRET histograms suggest the

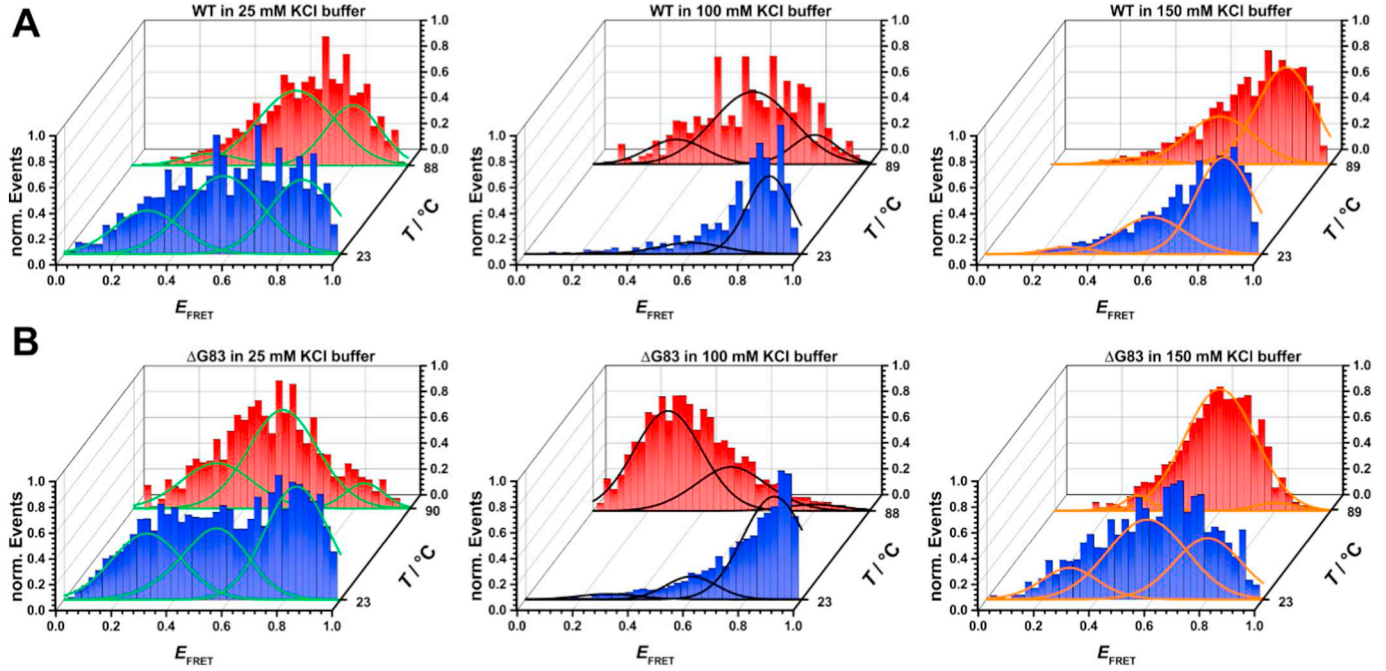

Fig. 8. FRET efficiency histograms and corresponding Gaussian fits of (A) microROSE WT and (B) ΔG83 in buffers of different KCl concentration at ambient (~20 °C, blue) and high temperature (~80 °C, red). The different shapes and positions of the histograms indicate changes in the distribution of conformers of the two hairpins. (For interpretation of the references to colour in this figure legend, the reader is referred to the web version of this article.)

occurrence of a high and a low E_{FRET} species. However, in the majority of measurements, intermediate states with medium E_{FRET} were observed. Hence, the histograms were fitted to a trimodal Gaussian distribution representing a closed conformation (high E_{FRET}), partially unfolded species (medium E_{FRET}) and an open conformation (low E_{FRET}). The peak centers were determined from histograms in which one of the three conformers was predominant.

3.3.1. Salt concentration effect

At low salt concentration (c_{KCl} = 25 mM), a broad distribution of conformers is observable both at low and high temperatures (Fig. 8). This is probably due to the repulsive interactions between neighboring negatively charged phosphate groups, which are not fully screened by the K^+ ions at that low salt concentration. In contrast, in the 100 mM KCl solution, the majority of the RNA molecules are in a conformation with a high-FRET efficiency, corresponding to the closed folded state, at low temperature. At high temperature, the distribution broadens, but is not entirely shifted to the low E_{FRET} states that represent the open unfolded conformation of the hairpin (Fig. 9, top, black dots). The histogram of the mutant is shifted to slightly different E_{FRET} values, in particular in the temperature-unfolded state, suggesting slightly different conformational states. At high temperature, increasing levels of KCl rescue the more compact conformational state.

Remarkably, increasing the salt concentration beyond physiological conditions (c_{KCl} = 150 mM) seems to have a destabilizing effect. This might be due to the accompanying increase of the Cl^- ion concentration in the ion atmosphere of the hairpin. MD simulations showed that chloride ions favorably interact with unfolded RNA molecules. Hence, the population of expanded conformations is promoted [74]. The destabilizing effect seems to be slightly more pronounced for the ΔG83 mutant. In a 3D view created from NMR structural data, geometrical changes of the RNA helix caused by the depletion of G83 became visible (Fig. 10). Helix bending results in modifications of the shape of the major groove. For instance, the distance between the two facing phosphate groups C77-**P**-A78 and A92-**P**-G91 is decreased from 17.1 Å to 12.9 Å (calculated from PDB: 2GIO, 2GIP [65]). The narrowing of the major groove in the mutant helix could cause a decreased accessibility to hydration water and counter ions, resulting in increased repulsive interactions of facing phosphate groups.

3.3.2. Osmolyte effects

Based on these findings, we then investigated the effect of the naturally occurring osmolytes TMAO and glycine on the conformational dynamics of the WT microROSE RNA hairpin in 100 mM KCl, i.e., at a salt concentration for which maximal stability of the RNA hairpin was observed. The effect of both osmolytes on the conformational dynamics is clearly visible (Fig. 11). In comparison to the neat 100 mM KCl buffer solution, the population of the folded high E_{FRET} state is more favorable at high temperature in the presence of both osmolytes. At ambient temperature, the percentage of the high E_{FRET} conformer is slightly smaller, while the percentage of the other two conformational states has increased in the presence of both osmolytes (Fig. 11). At high temperature, the high E_{FRET} state is more favorable in the presence of TMAO, while glycine still promotes the formation of medium E_{FRET} conformers. Overall, the two osmolytes render the population distribution less temperature sensitive. Though there is evidence that TMAO has a slight destabilizing effect on RNA secondary structures [8], we observe stabilization against heat-induced unfolding, which is in good agreement with our previous studies on the 4 U RNA hairpin [38]. A destabilizing effect of glycine at ambient temperature was also shown for a DNA hairpin, recently [46]. Lambert et al. found a general destabilizing effect of several osmolytes on the secondary structure of RNAs, explained by preferential interactions of the osmolyte with the nucleobases that get exposed upon unfolding [41]. Our findings suggest that those interactions already take place at rather low temperatures for the RNA thermometer.

3.3.3. Crowding effect

To mimic the high concentration of macromolecules in the cytoplasm, we selected the common macromolecular crowding agent Ficoll. The smFRET efficiency histograms show that Ficoll has a drastic effect on the conformational distribution of the RNA hairpin (Fig. 12A). The addition of Ficoll markedly decreases the percentage of the high-E_{FRET} conformer at ambient temperature by increasing the population of

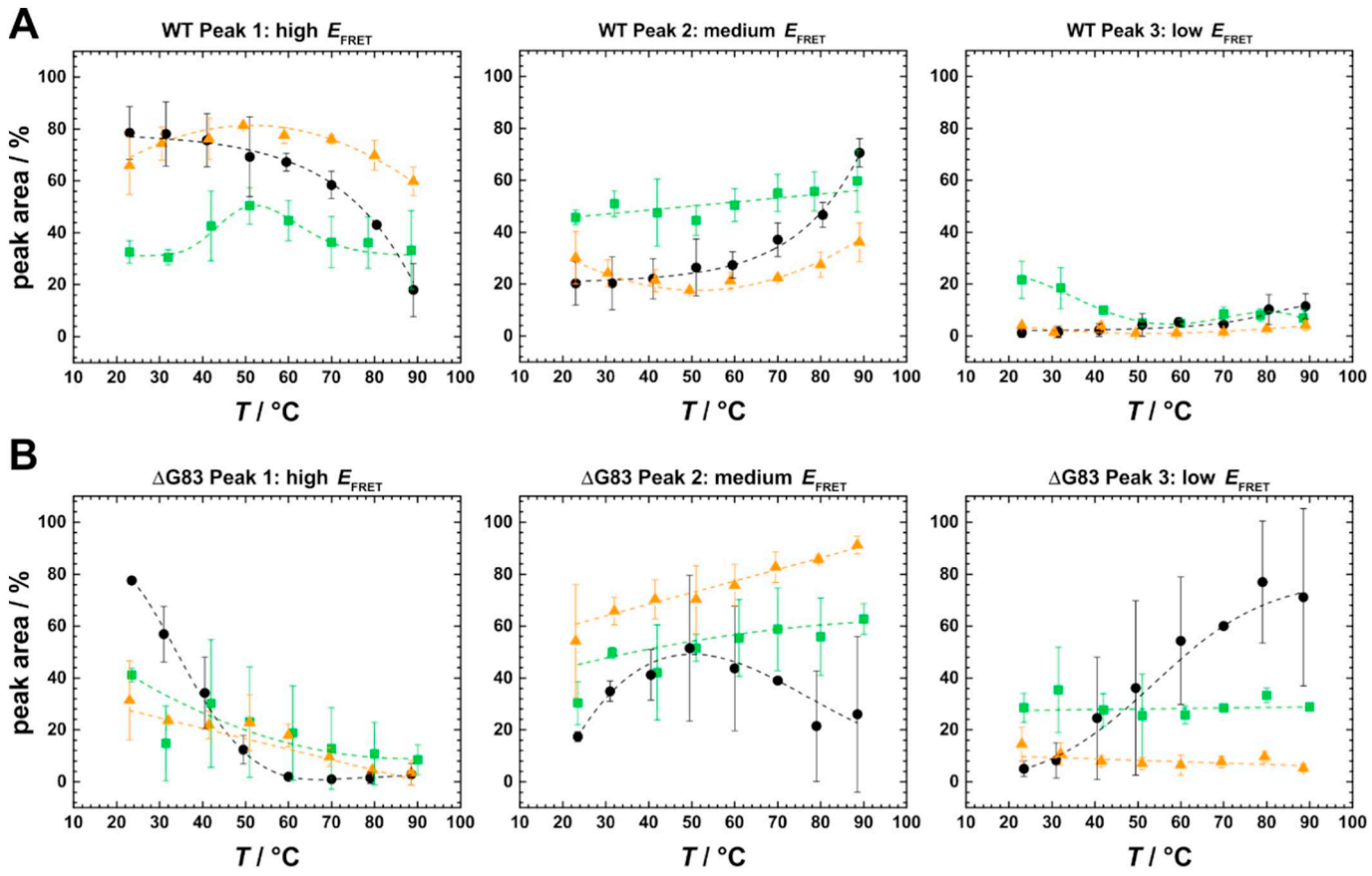

Fig. 9. Analysis of the FRET efficiency histograms of the microROSE hairpin. Temperature dependence of the peak areas corresponding to different conformational states. (A) WT and (B) ΔG83 mutant. Black dots: c_{KCl} = 100 mM; green squares: c_{KCl} = 25 mM; orange triangles: c_{KCl} = 150 mM. (For interpretation of the references to colour in this figure legend, the reader is referred to the web version of this article.)

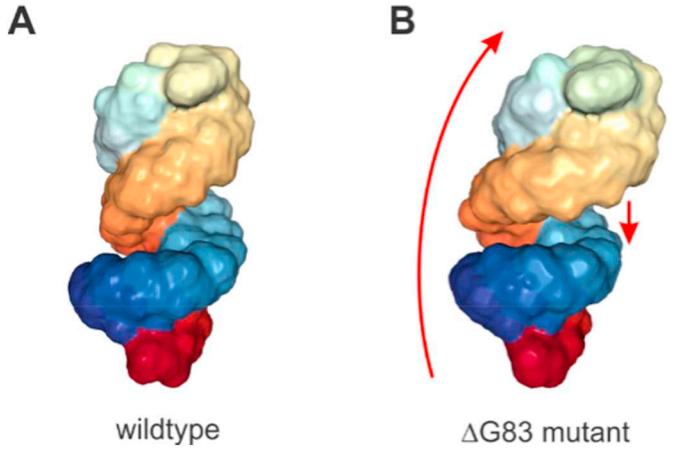

Fig. 10. 3D view of the microROSE hairpin [75]; (A) wildtype, (B) ΔG83 mutant. Depletion of G83 causes bending of the helix and modifies the shape of the major groove. PDB: 2GIO, 2GIP [65].

medium and low-E_{FRET} conformers compared to the neat buffer solution. Obviously, enthalpic ("quinary") interactions dominate the crowding effect, which could be due to favorable interactions between the ribose sugars (hydroxyl groups) and/or the nucleobases of the RNA and the sugar residues of Ficoll. This interpretation is supported by additional measurements using sucrose, the monomeric unit of the polysaccharide (Fig. 12). At high temperature, low-E_{FRET} conformers become favored, which suggests a high affinity of sucrose to the nucleobases that get exposed at higher temperatures. Compared to Ficoll, the effect of sucrose is more pronounced owing to the lower accessibility of the hydroxyl groups of the coiled polymer. Hence, the mode of action of Ficoll in this case is determined by enthalpically driven interactions. Likewise, Gao et al. observed a destabilizing effect of Ficoll and sucrose on a RNA secondary structure. In ensemble FRET measurements of the lm-4 U RNA hairpin melting, they found decreased ΔG_u^o values in the presence of crowding agents, which are explained by a decreased water activity of the solutions studied and attractive interactions between the cosolutes and the nucleobases that counteract the stabilizing excluded volume effect [35].

4. Conclusions

Our single-molecule FRET studies on three different types of nucleic acid fragments yielded new insights into how different solution conditions, including salts, osmolytes and crowding agents, are able to affect the distribution of conformers at different pressures and temperatures. Such information is not accessible from ensemble techniques which provide access to average structural properties, only. To mimic parts of the complex composition of the cellular milieu, we have chosen representatives of three classes of cellular background molecules that differ in size and chemical properties, i.e. inorganic salts, organic osmolytes and a macromolecular crowding agent. We could show that the conformational equilibrium of the RNA hairpin is highly susceptible to variations of the concentration of inorganic salts. Previous studies on a DNA hairpin revealed that even small concentration changes of counterions can have a significant impact and that the divalent Mg^{2+} ions are more potent in stabilizing closed conformations than the monovalent K^+ ions [4]. The supply of the appropriate amount of counterions in the cytosol is thus vital for effective screening of the negative

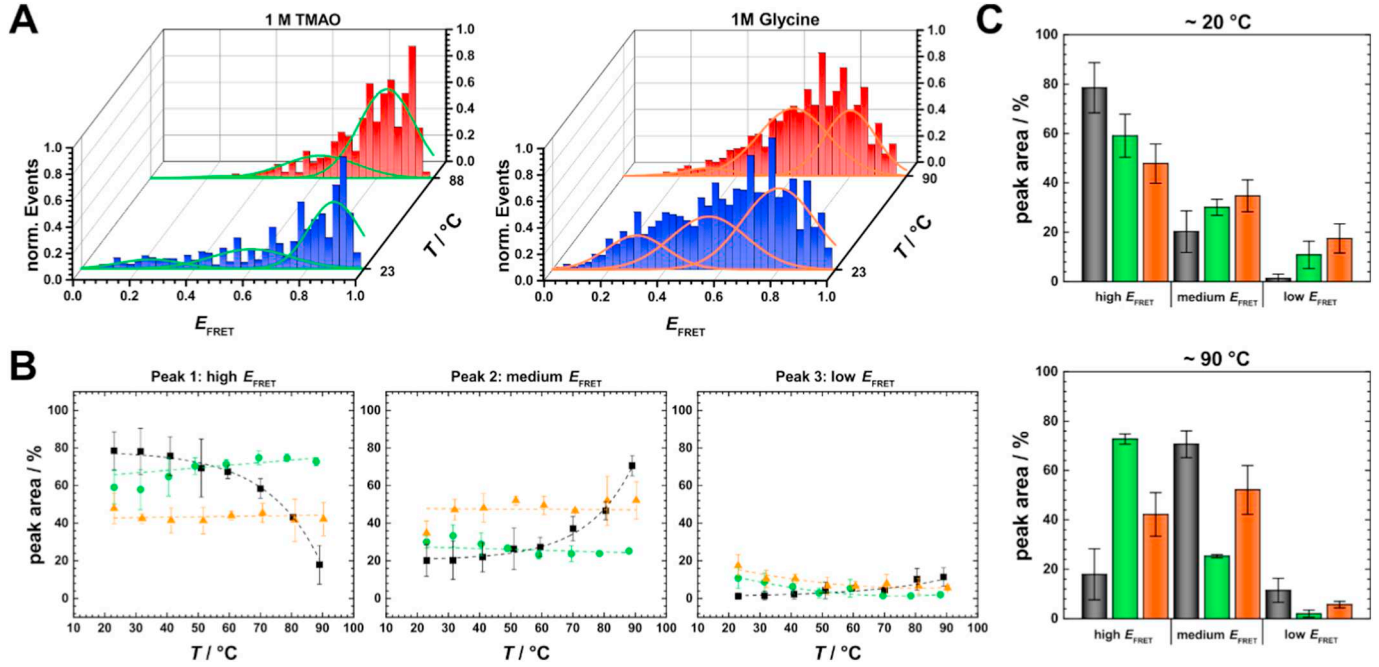

Fig. 11. FRET efficiency histograms and corresponding Gaussian fits for the microROSE WT in the presence of the osmolytes TMAO and glycine. (B) Peak analysis of the histograms shown in (A). The peak areas attributed to three different conformers are shown as a function of temperature. Black squares: reference (neat 100 mM KCl buffer); green dots: 1 M TMAO; orange triangles: 1 M glycine. (C) Peak areas related to the population of the three different conformers of microROSE WT in the presence of TMAO (green) and glycine (orange) at ambient and high temperature. Compared to the reference, the population of the folded high-E_{FRET} state is more favorable at high temperature in the presence of both osmolytes. (For interpretation of the references to colour in this figure legend, the reader is referred to the web version of this article.)

charge density of the phosphate backbone. The organic osmolyte TMAO, well known for its stabilizing effect on proteins, effectively stabilizes the nucleic acids under investigation against the deleterious effects of high pressures, high temperatures and urea, suggesting a universal mode of action. We surmise that unfavorable interactions between TMAO and the backbone phosphate groups shift the conformational equilibria to the compact low-SASA species. For the macromolecular crowding agent Ficoll, the mechanism seems to be less universal. For the DNA fragments (DNA hairpin [4], G-quadruplex) the strong excluded volume effect of Ficoll prevails and thus conformations

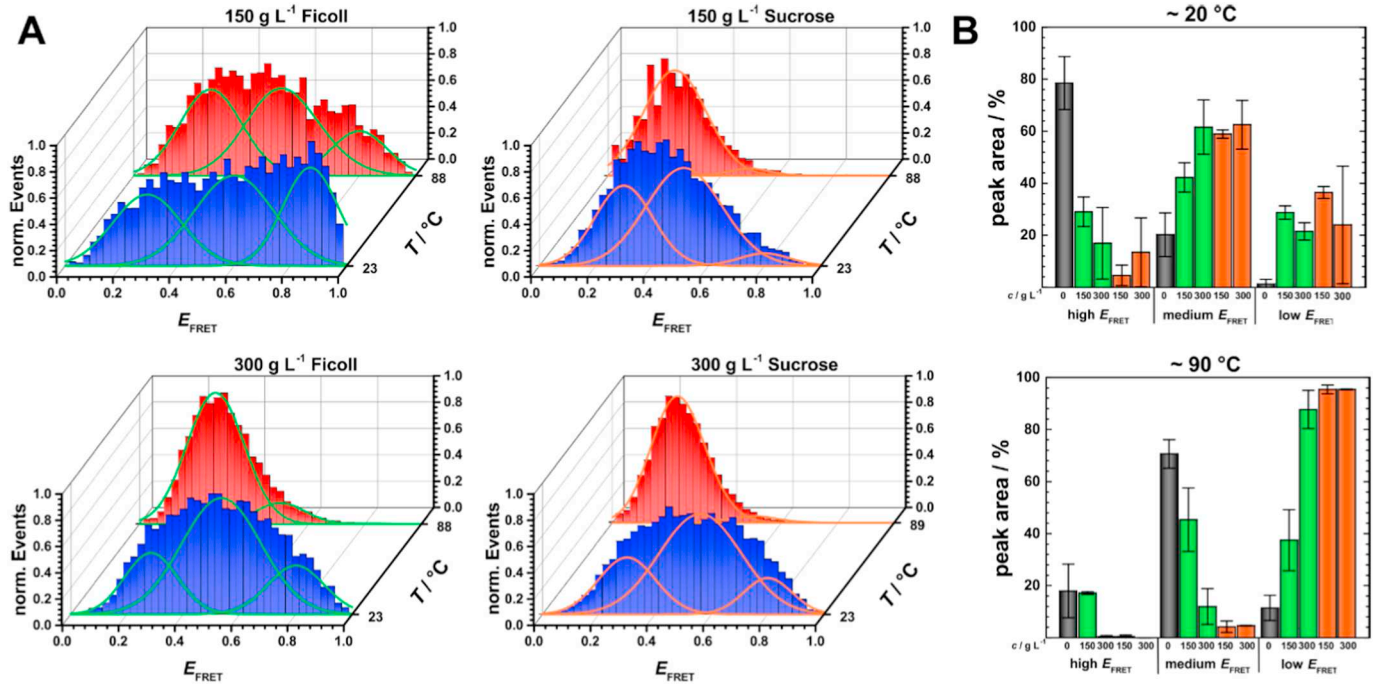

Fig. 12. FRET efficiency histograms and corresponding Gaussian fits of microROSE WT in the presence of 150 and 300 mg/mL Ficoll and sucrose. (B) Peak areas related to the population of the three different conformers of the microROSE WT RNA hairpin in the presence of Ficoll (green) and sucrose (orange) at ambient and high temperature. Both additives exhibit a strong destabilizing effect on the closed hairpin conformation and promote the population of medium- and high-E_{FRET} states at ambient and low temperature. (For interpretation of the references to colour in this figure legend, the reader is referred to the web version of this article.)

with lower SASA and volumes are favored. In case of the RNA hairpin, Ficoll promotes the formation of (partly) unfolded conformers, i.e. does not serve as inert crowding agent. The differences in the chemical structures of RNAs in comparison to DNAs (uracil instead of thymine and an additional hydroxyl group of the ribose sugar), creating different helix geometries and surface structures, are presumably responsible for the distinct interaction properties observed. Furthermore, the comparative study with the mutated RNA hairpin reveals the susceptibility of the conformational dynamics to the deletion of a single nucleobase. Such mutations can cause severe consequences in cellular processes that are regulated by conformational transitions like, in this particular case, the thermosensing by an mRNA.

Notes

The research was conducted in the absence of any commercial or financial relationships that could be construed as a potential conflict of interest.

Acknowledgements

Financial support from the DFG Research Unit FOR 1979 and in part by the Cluster of Excellence RESOLV (Deutsche Forschungsgemeinschaft (DFG, German Research Foundation) under Germany's Excellence Strategy, EXC-2033, Projektnummer 39067787) is gratefully acknowledged.

References

[1] P.H. Yancey, J.F. Siebenaller, Co-evolution of proteins and solutions: protein adaptation versus cytoprotective micromolecules and their roles in marine organisms, J. Exp. Biol. 218 (2015) 1880–1896, https://doi.org/10.1242/jeb.114355.
[2] S. Patra, N. Erwin, R. Winter, Translational dynamics of lipidated Ras proteins in the presence of crowding agents and compatible osmolytes, ChemPhysChem. 17 (2016) 2164–2169, https://doi.org/10.1002/cphc.201600179.
[3] D. De Sancho, A. Sirur, R.B. Best, Molecular origins of internal friction effects on protein-folding rates, Nat. Commun. 5 (2014) 1–10, https://doi.org/10.1038/ncomms5307.
[4] S. Patra, V. Schuabb, I. Kiesel, J.-M. Knop, R. Oliva, R. Winter, Exploring the effects of cosolutes and crowding on the volumetric and kinetic profile of the conformational dynamics of a poly dA loop DNA hairpin: a single-molecule FRET study, Nucleic Acids Res. 47 (2019) 981–996, https://doi.org/10.1093/nar/gky1122.
[5] B.P. Paudel, D. Rueda, Molecular crowding accelerates ribozyme docking and catalysis, J. Am. Chem. Soc. 136 (2014) 16700–16703, https://doi.org/10.1021/ja5073146.
[6] M. Tabaka, T. Kalwarczyk, J. Szymanski, S. Hou, R. Holyst, The effect of macromolecular crowding on mobility of biomolecules, association kinetics, and gene expression in living cells, Front. Phys. 2 (2014) 1–14, https://doi.org/10.3389/fphy.2014.00054.
[7] A. Soranno, I. Koenig, M.B. Borgia, H. Hofmann, F. Zosel, D. Nettels, B. Schuler, Single-molecule spectroscopy reveals polymer effects of disordered proteins in crowded environments, Proc. Natl. Acad. Sci. 111 (2014) 4874–4879, https://doi.org/10.1073/pnas.1322611111.
[8] D. Lambert, D. Leipply, D.E. Draper, The osmolyte TMAO stabilizes native RNA tertiary structures in the absence of Mg2+: evidence for a large barrier to folding from phosphate dehydration, J. Mol. Biol. 404 (2010) 138–157, https://doi.org/10.1016/j.jmb.2010.09.043.
[9] E.D. Holmstrom, N.F. Dupuis, D.J. Nesbitt, Kinetic and thermodynamic origins of osmolyte-influenced nucleic acid folding, J. Phys. Chem. B 119 (2015) 3687–3696, https://doi.org/10.1021/jp512491n.
[10] S. Bezrukavnikov, A. Mashaghi, R.J. van Wijk, C. Gu, L.J. Yang, Y.Q. Gao, S.J. Tans, Trehalose facilitates DNA melting: a single-molecule optical tweezers study, Soft Matter 10 (2014) 7269, https://doi.org/10.1039/C4SM01532K.
[11] E.A. Oprzeska-Zingrebe, M. Kohagen, J. Kästner, J. Smiatek, Unfolding of DNA by co-solutes: insights from Kirkwood–Buff integrals and transfer free energies, Eur. Phys. J. Spec. Top. 227 (2019) 1665–1679, https://doi.org/10.1140/epjst/e2019-800163-5.
[12] S. Flock, R. Labarbe, C. Houssier, 23Na NMR study of the effect of organic osmolytes on DNA counterion atmosphere, Biophys. J. 71 (1996) 1519–1529, https://doi.org/10.1016/S0006-3495(96)79354-2.
[13] F.C. Marincola, M. Casu, G. Saba, A. Lai, P. del Vecchio, G. Barone, A 23Na NMR study of the effect of d(+) and l(−) arabitol on NaDNA in aqueous solution, Int. J. Biol. Macromol. 29 (2001) 237–241, https://doi.org/10.1016/S0141-8130(01)00174-X.
[14] J. Hong, M.W. Capp, C.F. Anderson, R.M. Saecker, D.J. Felitsky, M.W. Anderson, M.T. Record, Preferential interactions of glycine betaine and of urea with DNA: implications for DNA hydration and for effects of these solutes on DNA stability, Biochemistry. 43 (2004) 14744–14758, https://doi.org/10.1021/bi049096q.
[15] L.J. Nordstrom, C.A. Clark, B. Andersen, S.M. Champlin, J.J. Schwinefus, Effect of ethylene glycol, urea, and N-methylated glycines on DNA thermal stability: the role of DNA base pair composition and hydration, Biochemistry. 45 (2006) 9604–9614, https://doi.org/10.1021/bi052469i.
[16] R.B. Macgregor, The interactions of nucleic acids at elevated hydrostatic pressure, Biochim. Biophys. Acta Protein Struct. Mol. Enzymol. 1595 (2002) 266–276, https://doi.org/10.1016/S0167-4838(01)00349-1.
[17] A. Kumar, Alternate view on thermal stability of the DNA duplex, Biochemistry. 34 (1995) 12921–12925, https://doi.org/10.1021/bi00040a001.
[18] E. Girard, T. Prange, A.-C. Dhaussy, E. Migianu-Griffoni, M. Lecouvey, J.-C. Chervin, M. Mezouar, R. Kahn, R. Fourme, Adaptation of the base-paired double-helix molecular architecture to extreme pressure, Nucleic Acids Res. 35 (2007) 4800–4808, https://doi.org/10.1093/nar/gkm511.
[19] R.B. Macgregor, Effect of hydrostatic pressure on nucleic acids, Biopolymers. 48 (1998) 253, https://doi.org/10.1002/(SICI)1097-0282(1998)48:4<253::AID-BIP5>3.0.CO;2-F.
[20] D.J. Wilton, M. Ghosh, K.V.A. Chary, K. Akasaka, M.P. Williamson, Structural change in a B-DNA helix with hydrostatic pressure, Nucleic Acids Res. 36 (2008) 4032–4037, https://doi.org/10.1093/nar/gkn350.
[21] J. Norberg, L. Nilsson, Constant pressure molecular dynamics simulations of the dodecamers: d (GCGCGCGCGCGC) 2 and r (GCGCGCGCGCGC) 2, J. Chem. Phys. 104 (1996) 6052–6057, https://doi.org/10.1063/1.471341.
[22] J. Barciszewski, J. Jurczak, S. Porowski, T. Specht, V.A. Erdmann, The role of water structure in conformational changes of nucleic acids in ambient and high-pressure conditions, Eur. J. Biochem. 260 (2001) 293–307, https://doi.org/10.1046/j.1432-1327.1999.00184.x.
[23] A. Krzyzaniak, P. Sałański, J. Jurczak, J. Barciszewski, B-Z DNA reversible conformation changes effected by high pressure, FEBS Lett. 279 (1991) 1–4 http://www.ncbi.nlm.nih.gov/pubmed/1995328.
[24] S. Takahashi, N. Sugimoto, Pressure-dependent formation of i-motif and G-quadruplex DNA structures, Phys. Chem. Chem. Phys. 17 (2015) 31004–31010, https://doi.org/10.1039/C5CP04727G.
[25] S. Takahashi, N. Sugimoto, Effect of pressure on thermal stability of G-quadruplex DNA and double-stranded DNA structures, Molecules. 18 (2013) 13297–13319, https://doi.org/10.3390/molecules181113297.
[26] H.Y. Fan, Y.L. Shek, A. Amiri, D.N. Dubins, H. Heerklotz, R.B. Macgregor, T.V. Chalikian, Volumetric characterization of sodium-induced G-quadruplex formation, J. Am. Chem. Soc. 133 (2011) 4518–4526, https://doi.org/10.1021/ja110495c.
[27] A.R. Amiri, R.B. Macgregor, The effect of hydrostatic pressure on the thermal stability of DNA hairpins, Biophys. Chem. 156 (2011) 88–95, https://doi.org/10.1016/j.bpc.2011.02.001.
[28] A.E. Garcia, D. Paschek, Simulation of the pressure and temperature folding/unfolding equilibrium of a small RNA hairpin, J. Am. Chem. Soc. 130 (2008) 815–817, https://doi.org/10.1021/ja074191i.
[29] M.S. Cheung, D. Klimov, D. Thirumalai, Molecular crowding enhances native state stability and refolding rates of globular proteins, Proc. Natl. Acad. Sci. 102 (2005) 4753–4758.
[30] A.P. Minton, Models for excluded volume interaction between an unfolded protein and rigid macromolecular cosolutes: macromolecular crowding and protein stability revisited, Biophys. J. 88 (2005) 971–985, https://doi.org/10.1529/biophysj.104.050351.
[31] I.M. Kuznetsova, K.K. Turoverov, V.N. Uversky, What macromolecular crowding can do to a protein, Int. J. Mol. Sci. 15 (2014) 23090–23140, https://doi.org/10.3390/ijms151223090.
[32] S.B. Zimmerman, A.P. Minton, Macromolecular crowding: biochemical, biophysical, and physiological consequences, Annu. Rev. Biophys. Biomol. Struct. 22 (1993) 27–65.
[33] P.H. Yancey, Organic osmolytes as compatible, metabolic and counteracting cytoprotectants in high osmolarity and other stresses, J. Exp. Biol. 208 (2005) 2819–2830, https://doi.org/10.1242/jeb.01730.
[34] D.R. Canchi, A.E. García, Cosolvent effects on protein stability, Annu. Rev. Phys. Chem. 64 (2013) 273–293, https://doi.org/10.1146/annurev-physchem-040412-110156.
[35] M. Gao, D. Gnutt, A. Orban, B. Appel, F. Righetti, R. Winter, F. Narberhaus, S. Müller, S. Ebbinghaus, RNA hairpin folding in the crowded cell, Angew. Chem. Int. Ed. 55 (2016) 3224–3228, https://doi.org/10.1002/anie.201510847.
[36] S. Patra, C. Anders, N. Erwin, R. Winter, Osmolyte effects on the conformational dynamics of a DNA hairpin at ambient and extreme environmental conditions, Angew. Chem. Int. Ed. 56 (2017) 5045–5049, https://doi.org/10.1002/anie.201701420.
[37] J.-M. Knop, S. Patra, B. Harish, C.A. Royer, R. Winter, The Deep Sea Osmolyte trimethylamine N -oxide and macromolecular crowders rescue the antiparallel conformation of the human telomeric G-quadruplex from urea and pressure stress, Chem. - A Eur. J. 24 (2018) 14346–14351, https://doi.org/10.1002/chem.201802444.
[38] M. Gao, L. Arns, R. Winter, Modulation of the thermodynamic signatures of an RNA thermometer by osmolytes and salts, Angew. Chem. Int. Ed. 56 (2017) 2302–2306, https://doi.org/10.1002/anie.201611843.
[39] N.F. Dupuis, E.D. Holmstrom, D.J. Nesbitt, Molecular-crowding effects on single-molecule RNA folding/unfolding thermodynamics and kinetics, Proc. Natl. Acad. Sci. 111 (2014) 8464–8469, https://doi.org/10.1073/pnas.1316039111.
[40] S.I. Nakano, D. Miyoshi, N. Sugimoto, Effects of molecular crowding on the structures, interactions, and functions of nucleic acids, Chem. Rev. 114 (2014) 2733–2758, https://doi.org/10.1021/cr400113m.

[41] D. Lambert, D.E. Draper, Effects of osmolytes on RNA secondary and tertiary structure stabilities and RNA-Mg2+ interactions, J. Mol. Biol. 370 (2007) 993–1005, https://doi.org/10.1016/j.jmb.2007.03.080.
[42] B. Schuler, E.A. Lipman, W.A. Eaton, Probing the free-energy surface for protein folding with single-molecule fluorescence spectroscopy, Nature. 419 (2002) 743–748, https://doi.org/10.1038/nature01062.1.
[43] A.A. Deniz, M. Dahan, J.R. Grunwell, T. Ha, A.E. Faulhaber, D.S. Chemla, S. Weiss, P.G. Schultz, Single-pair fluorescence resonance energy transfer on freely diffusing molecules: observation of Forster distance dependence and subpopulations, Proc. Natl. Acad. Sci. 96 (2002) 3670–3675, https://doi.org/10.1073/pnas.96.7.3670.
[44] S. Ruettinger, V. Buschmann, B. Kraemer, S. Orthaus, F. Koberling, FRET Analysis with Pulsed Interleaved Excitation (PIE) Using the MicroTime 200, (2013), pp. 1–8 https://www.picoquant.com/images/uploads/page/files/7266/appnote_pie-fret.pdf.
[45] B.K. Müller, E. Zaychikov, C. Bräuchle, D.C. Lamb, Pulsed interleaved excitation, Biophys. J. 89 (2005) 3508–3522, https://doi.org/10.1529/biophysj.105.064766.
[46] S. Patra, C. Anders, P.H. Schummel, R. Winter, Antagonistic effects of natural osmolyte mixtures and hydrostatic pressure on the conformational dynamics of a DNA hairpin probed at the single-molecule level, Phys. Chem. Chem. Phys. 20 (2018) 13159–13170, https://doi.org/10.1039/C8CP00907D.
[47] E. Sisamakis, A. Valeri, S. Kalinin, P.J. Rothwell, C.A.M. Seidel, Accurate single-molecule FRET studies using multiparameter fluorescence detection, Methods Enzymol. 475 (2010) 455–514, https://doi.org/10.1016/S0076-6879(10)75018-7.
[48] P.H. Yancey, W.R. Blake, J. Conley, Unusual organic osmolytes in deep-sea animals: adaptations to hydrostatic pressure and other perturbants, Comp. Biochem0. Phys. A. 133 (2002) 667–676, https://doi.org/10.1016/S1095-6433(02)00182-4.
[49] L.E. Baltierra-Jasso, M.J. Morten, L. Laflör, S.D. Quinn, S.W. Magennis, Crowding-induced hybridization of single DNA hairpins, J. Am. Chem. Soc. 137 (2015) 16020–16023, https://doi.org/10.1021/jacs.5b11829.
[50] R. Tippana, W. Xiao, S. Myong, G-quadruplex conformation and dynamics are determined by loop length and sequence, Nucleic Acids Res. 42 (2014) 8106–8114, https://doi.org/10.1093/nar/gku464.
[51] E.Y.N. Lam, D. Beraldi, D. Tannahill, S. Balasubramanian, G-quadruplex structures are stable and detectable in human genomic DNA, Nat. Commun. 4 (2013), https://doi.org/10.1038/ncomms2792.
[52] B.G. Kim, H.M. Evans, D.N. Dubins, T.V. Chalikian, Effects of salt on the stability of a G-quadruplex from the human c-MYC promoter, Biochemistry. 54 (2015) 3420–3430, https://doi.org/10.1021/acs.biochem.5b00097.
[53] A. Fujiwara, M. Fujiwara, C. Nishida-Umehara, S. Abe, T. Masaoka, Characterization of Japanese flounder karyotype by chromosome bandings and fluorescence in situ hybridization with DNA markers, Genetica. 131 (2007) 267–274, https://doi.org/10.1007/s10709-006-9136-z.
[54] S. Takahashi, N. Sugimoto, Effect of pressure on the stability of G-quadruplex DNA: thermodynamics under crowding conditions, Angew. Chem. Int. Ed. 52 (2013) 13774–13778, https://doi.org/10.1002/anie.201307714.
[55] J. Zhou, H. Tateishi-Karimata, J.L. Mergny, M. Cheng, Z. Feng, D. Miyoshi, N. Sugimoto, C. Li, Reevaluation of the stability of G-quadruplex structures under crowding conditions, Biochimie. 121 (2016) 204–208, https://doi.org/10.1016/j.biochi.2015.12.012.
[56] S. Takahashi, S. Bhowmik, N. Sugimoto, Volumetric analysis of formation of the complex of G-quadruplex DNA with hemin using high pressure, J. Inorg. Biochem. 166 (2016) 199–207, https://doi.org/10.1016/j.jinorgbio.2016.08.011.
[57] K.W. Lim, V.C.M. Ng, N. Martín-Pintado, B. Heddi, A.T. Phan, Structure of the human telomere in Na+ solution: an antiparallel (2+2) G-quadruplex scaffold reveals additional diversity, Nucleic Acids Res. 41 (2013) 10556–10562, https://doi.org/10.1093/nar/gkt771.
[58] S.L. Noer, S. Preus, D. Gudnason, M. Aznauryan, J.-L. Mergny, V. Birkedal, Folding dynamics and conformational heterogeneity of human telomeric G-quadruplex structures in Na + solutions by single molecule FRET microscopy, Nucleic Acids Res. 44 (2016) 464–471, https://doi.org/10.1093/nar/gkv1320.
[59] T. Fujii, P. Podbevšek, J. Plavec, N. Sugimoto, Effects of metal ions and cosolutes on G-quadruplex topology, J. Inorg. Biochem. 166 (2017) 190–198, https://doi.org/10.1016/j.jinorgbio.2016.09.001.
[60] M.C. Miller, R. Buscaglia, J.B. Chaires, A.N. Lane, J.O. Trent, Hydration is a major determinant of the G-quadruplex stability and conformation of the human telomere 3' sequence of d (AG 3 (TTAG 3) 3). Supplementary Materials: Contents: Methods Figures Figure S3. TOCSY spectrum of htel22 in 50% D 2 O: 50% CD, J. Am. Chem. Soc. 132 (2010) 17105–17107, https://doi.org/10.1021/ja105259m.
[61] I. Son, Y.L. Shek, D.N. Dubins, T.V. Chalikian, Hydration changes accompanying helix-to-coil DNA transitions, J. Am. Chem. Soc. 136 (2014) 4040–4047, https://doi.org/10.1021/ja5004137.
[62] E.A. Oprzeska-Zingrebe, J. Smiatek, Preferential binding of urea to single-stranded DNA structures: a molecular dynamics study, Biophys. J. 114 (2018) 1551–1562, https://doi.org/10.1016/j.bpj.2018.02.013.
[63] L. Aslanyan, J. Ko, B.G. Kim, I. Vardanyan, Y.B. Dalyan, T.V. Chalikian, Effect of urea on G-quadruplex stability, J. Phys. Chem. B 121 (2017) 6511–6519, https://doi.org/10.1021/acs.jpcb.7b03479.
[64] S. Chowdhury, C. Ragaz, E. Kreuger, F. Narberhaus, Temperature-controlled structural alterations of an RNA thermometer, J. Biol. Chem. 278 (2003) 47915–47921, https://doi.org/10.1074/jbc.M306874200.
[65] S. Chowdhury, C. Maris, F.H.-T. Allain, F. Narberhaus, Molecular basis for temperature sensing by an RNA thermometer, EMBO J. 25 (2006) 2487–2497, https://doi.org/10.1038/sj.emboj.7601128.
[66] Q. Zou, B.J. Bennion, V. Daggett, K.P. Murphy, The molecular mechanism of stabilization of proteins by TMAO and its ability to counteract the effects of urea, J. Am. Chem. Soc. 124 (2002) 1192–1202, https://doi.org/10.1021/ja004206b.
[67] D. Bolen, I.V. Baskakov, The osmophobic effect: natural selection of a thermodynamic force in protein folding 1 1Edited by D. Draper, J. Mol. Biol. 310 (2001) 955–963, https://doi.org/10.1006/jmbi.2001.4819.
[68] D.L. Pincus, C. Hyeon, D. Thirumalai, Effects of trimethylamine N -oxide (TMAO) and crowding agents on the stability of RNA hairpins, J. Am. Chem. Soc. 130 (2008) 7364–7372, https://doi.org/10.1021/ja078326w.
[69] J.C. Miner, K. Hackett, Preferential interactions of K+/Cl− and TMAO with a model RNA oligomer, Biophys. J. 116 (2019), https://doi.org/10.1016/j.bpj.2018.11.1918 353a.
[70] M. Gao, C. Held, S. Patra, L. Arns, G. Sadowski, R. Winter, Crowders and cosolvents-major contributors to the cellular milieu and efficient means to counteract environmental stresses, ChemPhysChem. 18 (2017) 2951–2972, https://doi.org/10.1002/cphc.201700762.
[71] H.-X. Zhou, G. Rivas, A.P. Minton, Macromolecular crowding and confinement: biochemical, biophysical, and potential physiological consequences, Annu. Rev. Biophys. 37 (2008) 375–397, https://doi.org/10.1146/annurev.biophys.37.032807.125817.
[72] D. Kilburn, J.H. Roh, L. Guo, R.M. Briber, S.A. Woodson, Molecular crowding stabilizes folded RNA structure by the excluded volume effect, J. Am. Chem. Soc. 132 (2010) 8690–8696, https://doi.org/10.1021/ja101500g.
[73] E. Fiorini, R. Börner, R.K.O. Sigel, Mimicking the in vivo environment – the effect of crowding on RNA and biomacromolecular folding and activity, Chim. Int. J. Chem. 69 (2015) 207–212, https://doi.org/10.2533/chimia.2015.207.
[74] J.C. Miner, A.E. García, Concentration-dependent and configuration-dependent interactions of monovalent ions with an RNA tetraloop, J. Chem. Phys. 148 (2018) 222837, https://doi.org/10.1063/1.5019939.
[75] A.S. Rose, A.R. Bradley, Y. Valasatava, J.M. Duarte, A. Prlić, P.W. Rose, NGL viewer: web-based molecular graphics for large complexes, Bioinformatics. 34 (2018) 3755–3758, https://doi.org/10.1093/bioinformatics/bty419.